Identification of rare loss of function genetic variation regulating body fat distribution

Supplementary Materials

Table of Contents

Supplementary Table 1: Variants associated with waist-to-hip ratio adjusted for body mass index (WHR$_{adjBMI}$) in the discovery genome-wide analysis of rare non-synonymous variants.

Gene	dbSNP rsID	Genomic coordinate, chromosome and position	Effect allele and other allele	Effect allele frequency in % (minor allele count)	Protein change (amino acid corresponding to the effect allele)	Beta (SE) for WHR$_{adjBMI}$ per effect allele in univariate analysis, in SD units	p-value	Beta (SE) for WHR$_{adjBMI}$ per effect allele in conditional analyses[*], in SD units	p-value conditional analyses[*]
Sex-combined									
PLIN1	rs139271800	chr15:89671546	G and A	0.1 (1,127)	p.L90P (P)	-0.21 (0.029)	5.5×10^{-13}	-0.21 (0.029)	5.5×10^{-13}
PDE3B	rs150090666	chr11:14843853	T and C	0.1 (932)	p.R783X (X)	-0.26 (0.032)	1.4×10^{-15}	-0.25 (0.032)	6.2×10^{-15}
ACVR1C	rs56188432	chr2:157550353	G and A	0.2 (2,113)	p.I195T (T)	-0.14 (0.021)	4.9×10^{-11}	-0.14 (0.021)	5.4×10^{-12}
CALCRL	rs61739909	chr2:187380712	G and A	0.3 (2,954)	p.L87P (P)	-0.13 (0.018)	2.0×10^{-13}	-0.12 (0.018)	5.9×10^{-12}
ABHD15	rs141385558	chr17:29566527	T and C	0.3 (2,441)	p.G147D (D)	0.11 (0.019)	6.3×10^{-9}	0.07 (0.019)	0.00019
PYGM	rs116987552	chr11:64759751	A and G	0.4 (3,764)	p.R50X (X)	0.09 (0.016)	7.0×10^{-9}	0.06 (0.015)	0.00037
Sex-specific analysis in women ‡									
PLCB3	rs145502455	chr11:64263558	A and G	0.4 (2,028)	p.V806I (I)	0.13 (0.021)	1.6×10^{-10}	0.03 (0.020)	0.11
FNIP1	rs115209326	chr5:131672891	T and C	0.3 (1,655)	p.R518Q (Q)	-0.13 (0.023)	4.8×10^{-9}	-0.12 (0.023)	3.8×10^{-7}

Analyses are from 450,562 European ancestry individuals. Genomic coordinates according to human genome reference sequence hg38.

* Adjusting for conditionally-independent index variants highlighted in the joint conditional model (see Supplementary Table 3 for list of index variants at loci where fine-mapping supported causal role of these variants and Supplementary Table 4 for other loci).

‡ Variants in addition to the one of the sex-combined primary analysis which were identified in a secondary analysis in 244,478 women from the UK Biobank study ($p<5\times10^{-8}$).

Abbreviations: SE, standard error; WHR, waist-to-hip ratio; BMI, body mass index; SD, standard deviation.

Supplementary Table 2. a. Correlation between the UK Biobank WES data and the genotype data for rare nonsynonymous variants with a minor allele frequency (MAF) between 0.1% - 0.5% in overlapping samples. b. Rare allele concordance between the UK Biobank WES data and the genotype data for rare nonsynonymous variants with a MAF between 0.1% - 0.5% in overlapping samples.

a.

Min	1st Q	Median	Mean	3rd Q	Max
0.002	0.989	0.996	0.988	0.999	1

b.

Min	1st Q	Median	Mean	3rd Q	Max
0.002	0.991	0.997	0.987	0.999	1

Supplementary Table 3: a. Conditionally independent index variants and fine-mapping at the *CALCRL*, *PLIN1*, *PDE3B* and *ACVR1C* loci. Analyses are from 450,562 European ancestry individuals. Beta and standard errors are in standardized units of BMI-adjusted WHR per copy of the effect allele. Genomic coordinates according to human genome reference sequence GRCh38. **b. Formal conditional analyses at the *CALCRL, PLIN1, PDE3B* and *ACVR1C* loci.** Formal conditional analyses were conducted using individual-level genotype data in a subset of 350,721 unrelated European ancestry participants of UK Biobank. Because this is a subset of the discovery study, associations estimates differ from those presented in Supplementary Table 1.

a.

Locus	Signal	dbSNP rsID	Genomic coordinate, chromosome, position, effect allele, other allele (effect allele frequency, %)	Annotation	Beta (SE) from univariate analysis, in SD units	p-value univariate analysis	Beta (SE) from conditional analysis*, in SD units	p-value conditional analysis*	Genomic position of 99% credible set window, (width in number of base pairs)	Number of variants in the credible set	PPA for the index variant, %
PLIN1	1‡	rs139271800	chr15:89671546:G:A (0.1%)	*PLIN1* p.L90P	-0.21 (0.029)	5.5×10^{-13}	-0.21 (0.029)	5.5×10^{-13}	89671546 (1)	1	>99%
PDE3B	1‡	rs150090666	chr11:14843853:T:C (0.1%)	*PDE3B* p.R783X	-0.26 (0.032)	1.4×10^{-15}	-0.25 (0.032)	6.2×10^{-15}	14843853 (1)	1	>99%
	2	rs2970332	chr11:14338889:G: A (23.1%)	*RRAS2* intronic	-0.02 (0.002)	9.9×10^{-12}	-0.02 (0.002)	6.3×10^{-12}	14236464-14667794 (431,331)	20	23%
	3	rs79634051	chr11:14540399:C: G (2.8%)	*PSMA1* intronic	-0.03 (0.006)	6.4×10^{-8}	-0.04 (0.006)	2.1×10^{-9}	14221316-14869595 (648,280)	15	78%
ACVR1C	1	rs55920843	chr2:157556189:G: T (1.2%)	*ACVR1C* p.N150H	-0.08 (0.009)	8.9×10^{-19}	-0.09 (0.009)	4.6×10^{-20}	157556189 (1)	1	>99%
	2	rs2444770	chr2:157647227:C:T (14.8%)	18kb 5' of *ACVR1C*	-0.02 (0.003)	5.9×10^{-13}	-0.02 (0.003)	7.7×10^{-15}	157639990-157661726 (21,737)	7	46%
	3‡	rs56188432	chr2:157550353:G: A (0.2%)	*ACVR1C* p.I195T	-0.14 (0.021)	4.9×10^{-11}	-0.14 (0.021)	5.4×10^{-12}	157550353 (1)	1	>99%
CALCRL	1	rs10177093	chr2:187349092:G:T (45.6%)	*CALCRL* intronic	-0.02 (0.002)	2.2×10^{-27}	-0.02 (0.002)	7.7×10^{-26}	187223800-187349092 (125,293)	60	17%
	2‡	rs61739909	chr2:187380712:G: A (0.3%)	*CALCRL* p.L87P	-0.13 (0.018)	2.0×10^{-13}	-0.12 (0.018)	5.9×10^{-12}	187380712-187405532 (24,821)	2	51%

* Adjusting for conditionally-independent index variants highlighted in the joint conditional model.

‡ Variant identified in the genome-wide scan of rare nonsynonymous variants.

Abbreviations: SE, standard error; SD, standard deviation; PPA, posterior probability of association.

3

b.

Locus	Signal number	dbSNP rsID	Beta (SE) from univariate analysis	p-value univariate analysis	Beta (SE) from conditional analyses	p-value conditional analyses
CALCRL	1	rs10177093	-0.02 (0.002)	4.4×10^{-22}	-0.02 (0.002)	2.2×10^{-20}
	2	rs61739909	-0.15 (0.021)	9.8×10^{-13}	-0.14 (0.021)	5.5×10^{-11}
PLIN1	1	rs139271800	-0.16 (0.034)	2.3×10^{-6}	-0.16 (0.034)	2.3×10^{-6}
PDE3B	1	rs150090666	-0.24 (0.037)	2.0×10^{-11}	-0.24 (0.037)	1.7×10^{-10}
	2	rs2970332	-0.02 (0.003)	9.8×10^{-8}	-0.02 (0.003)	1.2×10^{-7}
	3	rs79634051	-0.03 (0.007)	2.9×10^{-5}	-0.03 (0.007)	2.0×10^{-6}
ACVR1C	1	rs55920843	-0.09 (0.011)	3.1×10^{-15}	-0.09 (0.011)	3.0×10^{-16}
	2	rs2444770	-0.02 (0.003)	2.8×10^{-10}	-0.02 (0.003)	1.7×10^{-11}
	3	rs56188432	-0.14 (0.025)	9.9×10^{-9}	-0.15 (0.025)	4.7×10^{-9}

Supplementary Table 4: Conditionally-independent index variants at the *ABHD15, PYGM, PLCB3 and FNIP1* regions.

Locus	dbSNP rsID	Chromosome and position
Sex-combined		
ABHD15	rs62070804	17: 29562625
ABHD15	rs561089333	17: 30422242
PYGM	rs224170	11: 63897410
PYGM	rs12419038	11: 64145264
PYGM	rs3751122	11: 64185649
PYGM	rs11231721	11: 64190363
PYGM	rs7952318	11: 64193770
PYGM	rs56271783	11: 64237251
PYGM	rs75152214	11: 64543641
PYGM	rs186402106	11: 64700853
PYGM	rs2306363	11: 65638129
PYGM	rs10750766	11: 65706327
PYGM	rs4645917	11: 65714169
PYGM	rs593982	11: 65745636
Sex-specific analysis in women †		
PLCB3	rs11231698	11: 64109691
PLCB3	rs3751122	11: 64185649
PLCB3	rs138055838	11: 64220169
PLCB3	rs56271783	11: 64237251
PLCB3	rs186826945	11: 64452647
FNIP1	rs74667082	5: 131412611

Conditional analyses estimated the association of each index variant while adjusting for all other index variants at the region. Index variants were selected using a joint meta-analysis model with GCTA [1].

† Identified in a secondary analysis in 244,478 women from the UK Biobank study ($p<5\times10^{-8}$).

Supplementary Table 5: STAAR-O [2] gene-based results for genes discovered in the single variant analysis.

Category	Gene	Number of Variants	Pval	Beta	SE
pLoF	*PLIN1*	31	9.82×10^{-9}	-0.27	0.05
Moderate	*PLIN1*	216	9.21×10^{-6}	-0.02	0.01
pLoF + Moderate	*PLIN1*	292	4.94×10^{-6}	-0.03	0.01
pLoF	*ACVR1C*	9	5.50×10^{-2}	-0.48	0.24
Moderate	*ACVR1C*	130	4.57×10^{-7}	-0.15	0.03
pLoF + Moderate	*ACVR1C*	139	1.68×10^{-7}	-0.15	0.03
pLoF	*PDE3B*	65	1.41×10^{-6}	-0.21	0.04
Moderate	*PDE3B*	392	8.12×10^{-2}	-0.007	0.01
pLoF + Moderate	*PDE3B*	437	2.26×10^{-5}	-0.03	0.01
pLoF	*CALCRL*	19	1.10×10^{-1}	0.31	0.14
Moderate	*CALCRL*	114	1.12×10^{-3}	-0.07	0.02
pLoF + Moderate	*CALCRL*	133	1.16×10^{-3}	-0.06	0.02

Abbreviations: pLOF, predicted loss of function; Pval, STAAR-O p-value; Beta, effect size; SE, standard error.

Supplementary Table 6: Significant gene-based results from the exome-wide scan for WHR$_{adjBMI}$.

Category	Gene	Number of variants	Genotype counts (RR/RA/AA)	Pval	Beta	SE
pLoF	*PLIN4*	65	183,900/1,065/0	5.86×10^{-7}	0.16	0.03
pLoF	*PLIN1*	31	184,572/388/5	9.82×10^{-9}	-0.27	0.05
pLoF	*INSR*	27	184,904/61/0	6.21×10^{-7}	-0.64	0.12
Moderate	*ACVR1C*	130	183,551/1,414/0	4.57×10^{-7}	-0.15	0.03
pLoF + Moderate	*ACVR1C*	139	183,535/1,430/0	1.68×10^{-7}	-0.15	0.03
pLoF	*PDE3B*	44	184,474/491/0	1.41×10^{-6}	-0.21	0.04

Abbreviations: pLOF, predicted loss of function; MAF, minor allele frequency; Pval, STAAR-O p-value; Beta, effect size; SE, standard error; RR, reference/reference genotype; RA, reference/alternate genotypes; AA, alternate/alternate genotypes.

Supplementary Table 7: Sex-specific results for gene-based analysis.

Gene			Women (n=101,569)			Men (n=82,677)		
Category	Gene	P_sexdiff	Beta	SE	Pval	Beta	SE	Pval
pLoF	*PLIN4*	2.08×10^{-2}	0.214	0.039	1.66×10^{-7}	0.073	0.046	1.55×10^{-1}
pLoF	*PLIN1*	2.83×10^{-1}	-0.330	0.065	8.96×10^{-8}	-0.223	0.075	4.56×10^{-3}
pLoF	*INSR*	4.62×10^{-7}	-1.218	0.168	1.44×10^{-12}	0.046	0.186	7.53×10^{-1}
Moderate	*ACVR1C*	1.13×10^{-1}	-0.181	0.035	7.78×10^{-7}	-0.098	0.039	5.28×10^{-2}
pLoF + Moderate	*ACVR1C*	1.22×10^{-1}	-0.183	0.034	4.60×10^{-7}	-0.103	0.039	4.03×10^{-2}
pLoF	*PDE3B*	1.85×10^{-3}	-0.334	0.059	5.04×10^{-8}	-0.057	0.067	1.87×10^{-1}

Abbreviations: pLOF, predicted loss of function; P_sexdiff, p-value for the significance of the difference in women and men beta values; Pval, STAAR-O p-value; Beta, effect size; SE, standard error; RR, reference/reference genotype; RA, reference/alternate genotypes; AA alternate/alternate genotypes.

Supplementary Table 8: Quality control measurements and annotation for variants included in the refined gene-based tests and single marker association results for all included variants. Annotations were performed using Variant Effect Predictor [3]. Single marker analyses were performed using the BOLT-LMM software [4].

[Excel file: Koprulu2021_WHRadjBMI_SupplementaryTable8.xlsx]

Abbreviations: CHROM: Chromosome; POS, position (GRCh38 [hg38]); REF, reference allele; ALT, alternative allele; IMPACT, the impact modifier for the consequence type; SYMBOL, the gene symbol; gene, Ensembl stable ID of affected gene; CADD_PHRED, CADD scores(phred-scaled); MAF, minor allele frequency; Consequence, consequence type of this variant; Protein_position, relative position of amino acid in protein; Amino_acids, only given if the variant affects the protein-coding sequence; biallelic_multiallelic, biallelic/multiallelic indicator; SIFT, the SIFT prediction and/or score, with both given as prediction(score); PolyPhen, the PolyPhen prediction and/or score; LOF, Loss-Of-Function Transcript Effect Estimator (LOFTEE) prediction; QUAL, Phred-scaled probability that the site has no variant; DP_MIN/MEAN/MAX, minimum/mean/maximum approximate read depth; GQ_MIN/MEAN/MAX, minimum/mean/maximum Genotype Quality; % allele imbalance, percentage of the imbalanced heterozygous calls; AA, number of homozygous reference alleles; AB, number of heterozygous calls; BB, number of homozygous alternative alleles; missing, number of missing calls; %missing, percentage of missing calls; MAC, minor allele counts; BETA, effect size; SE, standard error; P_BOLT_LMM, BOLT-LMM p-values for single marker test.

Supplementary Table 9: a. Summary statistics for quantitative traits from gene-based association analyses in sex-combined, women-only and male-only data. b. Summary statistics for binary traits from gene-based association analyses in sex-combined, women-only and male-only data. Details for all phenotypes and are given on Supplementary Table 12.

[Excel file: Koprulu2021_WHRadjBMI_SupplementaryTable9.xlsx]

Abbreviations: pLOF, predicted loss of function; Pval, STAAR-O p-value for phenotypic traits in Supplementary Table 9a and generalized linear model for binary traits Supplementary Table 9b; Beta, effect size; SE, standard error; Beta_LCI, lower 95% confidence interval for effect size in; Beta_UCI, upper 95% confidence interval for effect size; TG, triglyceride; HDL, high-density lipoprotein; LDL, low-density lipoprotein.

Supplementary Table 10: a. Lookup from theType 2 Diabetes Knowledge Portal for type 2 diabetes. Seven different masks were applied to filter the variants used in the association analysis: LofTee (predicted loss of function); 5/5 (predicted deleterious by 5 methods); 16/16 (predicted deleterious by 16 methods); 5/5 + LofTee LC (predicted deleterious by 5 methods, plus LofTee low confidence), 5/5 + 0/5 1% (variants predicted deleterious by 5 methods, plus variants with minor allele frequency < 1% that are not predicted to be deleterious by any of 5 methods); 5/5 + 1/5 1% (variants predicted deleterious by 5 methods, plus variants with minor allele frequency < 1% that are predicted to be deleterious by 1 of 5 methods); and 11/11 (predicted deleterious by 11 methods). Rows in bold have P-value ≤ 0.05. Accessed from https://t2d.hugeamp.org/ on 02/09/2021. **b. Lookup from AstraZeneca PheWAS Portal [5] for type 2 diabetes, non-insulin-dependent diabetes mellitus (Union#E11#E11) and chronic ischaemic heart disease (Union#I25#I25).** The variant categories used in collapsing models are provided in the parentheses in 'Collapsing Model' column. Rows in bold have P-value ≤ 0.05. Accessed from https://azphewas.com/ on 02/09/2021.

a.

Gene	Mask	P-value	Combined AF	Passing Variants	Singleton Variants	Standard Error	Sample Size	Odds Ratio
PLIN4	**LofTee**	**0.042**	**0.0042**	**17**	**6**	**0.153**	**43,125**	**1.3641**
PLIN4	**16/16**	**0.042**	**0.0042**	**17**	**6**	**0.153**	**43,125**	**1.3641**
PLIN4	**11/11**	**0.042**	**0.0042**	**17**	**6**	**0.153**	**43,125**	**1.3641**
PLIN4	5/5	0.907	0.0115	24	8	0.094	43,125	1.0110
PLIN4	5/5 + LofTee LC	0.907	0.0115	24	8	0.094	43,125	1.0110
PLIN4	5/5 + 1/5 1%	0.793	0.0350	174	59	0.051	43,125	1.0134
PLIN4	5/5 + 0/5 1%	0.653	0.0547	307	111	0.039	43,125	0.9825
PLIN1	11/11	0.478	0.0009	11	5	0.337	43,125	0.7905
PLIN1	5/5	0.237	0.0033	19	10	0.171	43,125	0.8178
PLIN1	5/5 + LofTee LC	0.237	0.0033	19	10	0.171	43,125	0.8178
PLIN1	5/5 + 1/5 1%	0.928	0.0121	87	39	0.089	43,125	0.9920
PLIN1	5/5 + 0/5 1%	0.678	0.0153	132	56	0.079	43,125	0.9679
INSR	**LofTee**	**0.017**	**0.0003**	**11**	**10**	**0.595**	**43,125**	**3.6645**
INSR	**16/16**	**0.015**	**0.0004**	**13**	**11**	**0.536**	**43,125**	**3.3304**
INSR	11/11	0.229	0.0008	24	18	0.343	43,125	1.4992
INSR	5/5	0.836	0.0012	32	24	0.282	43,125	1.0596
INSR	5/5 + LofTee LC	0.836	0.0012	32	24	0.282	43,125	1.0596
INSR	5/5 + 1/5 1%	0.814	0.0234	212	128	0.064	43,125	0.9850

INSR	5/5 + 0/5 1%	0.803	0.0284	251	145	0.058	43,125	0.9855
ACVR1C	LofTee	0.534	0.0000	2	2	2.112	43,125	0.3845
ACVR1C	16/16	0.056	0.0001	5	5	1.654	43,125	0.1131
ACVR1C	11/11	0.084	0.0019	14	10	0.240	43,125	0.6662
ACVR1C	5/5	0.053	0.0020	15	10	0.238	43,125	0.6380
ACVR1C	5/5 + LofTee LC	0.053	0.0020	15	10	0.238	43,125	0.6380
ACVR1C	5/5 + 1/5 1%	0.152	0.0127	67	40	0.090	43,125	0.8791
ACVR1C	5/5 + 0/5 1%	0.119	0.0132	79	47	0.089	43,125	0.8717
PDE3B	LofTee	0.562	0.0010	12	9	0.316	43,125	0.8349
PDE3B	16/16	0.678	0.0010	13	10	0.311	43,125	0.8802
PDE3B	11/11	0.739	0.0013	21	17	0.280	43,125	0.9118
PDE3B	5/5	0.847	0.0020	37	27	0.222	43,125	0.9584
PDE3B	5/5 + LofTee LC	0.766	0.0020	38	28	0.221	43,125	0.9369
PDE3B	5/5 + 1/5 1%	0.770	0.0238	178	98	0.064	43,125	0.9815
PDE3B	5/5 + 0/5 1%	0.829	0.0331	263	148	0.054	43,125	1.0116

b.

Gene	Phenotype	Collapsing model (Explanation)	P value	No. participants	No. cases with QV	No. controls with QV	Odds ratio	Odds ratio LCI	Odds ratio UCI
PLIN4	Type 2 diabetes	Synonymous negative control (synonymous variants with MAF≤0.05%)	8.69×10^{-2}	162,620	14	844	1.60	0.94	2.72
PLIN1	Type 2 diabetes	NA	NA	NA	NA	NA	NA	NA	NA
INSR	Type 2 diabetes	NA	NA	NA	NA	NA	NA	NA	NA
ACVR1C	Type 2 diabetes	Ultra-rare damaging (non-synonymous variants with MAF≤0.005%, REVEL score ≥ 0.25)	6.95×10^{-2}	162,620	3	89	3.25	1.03	10.28
PDE3B	Type 2 diabetes	Non-synonymous recessive (non-synonymous variants with MAF≤1%)	9.23×10^{-2}	162,620	3	101	2.86	0.91	9.04
PLIN1	Non-insulin-dependent diabetes mellitus (Union#E11#E11)	NA	NA	NA	NA	NA	NA	NA	NA
PLIN4	Non-insulin-dependent diabetes mellitus (Union#E11#E11)	NA	NA	NA	NA	NA	NA	NA	NA
INSR	Non-insulin-dependent diabetes mellitus (Union#E11#E11)	NA	NA	NA	NA	NA	NA	NA	NA
ACVR1C	Non-insulin-dependent diabetes mellitus (Union#E11#E11)	NA	NA	NA	NA	NA	NA	NA	NA
PDE3B	Non-insulin-dependent diabetes mellitus (Union#E11#E11)	Non-synonymous recessive (non-synonymous variants with MAF≤1%)	9.66×10^{-2}	201,921	18	107	1.54	0.94	2.54
PLIN4	Chronic ischaemic heart disease (Union#I25#I25)	NA	NA	NA	NA	NA	NA	NA	NA
PLIN1	**Chronic ischaemic heart disease (Union#I25#I25)**	Flexible MAF, damaging non-synonymous (non-synonymous variants with MAF≤0.1%, REVEL score ≥ 0.25)	2.67×10^{-2}	176170	48	424	0.71	0.53	0.96
		Flexible MAF, all non-synonymous (non-synonymous variants with MAF≤0.1%)	1.88×10^{-2}	176170	179	1355	0.83	0.71	0.97
		Flexible MAF, non-synonymous, Missense Tolerance Ratio (MTR) informed (non-synonymous variants with MAF≤0.1%, MTR <25th %ile or intergenic MTR < 50th %ile)	9.70×10^{-3}	176,170	88	740	0.75	0.60	0.93
		Protein truncating (protein truncating variants with MAF≤0.1%)	$\mathbf{4.49\times10^{-4}}$	**176,170**	**22**	**284**	**0.49**	**0.32**	**0.75**

		Protein truncating (protein truncating variants with MAF≤5%)	4.49×10^{-4}	176,170	22	284	0.49	0.32	0.75
		Protein truncating or rare damaging models combined (protein truncating variants with MAF≤5% and missense variants with MAF≤0.025% and REVEL score ≥ 0.25)	4.64×10^{-4}	176,170	32	369	0.55	0.38	0.78
PLIN1	Chronic ischaemic heart disease (Union#I25#I25)	Non-synonymous recessive (non-synonymous variants with MAF≤1%)	8.51×10^{-2}	176,170	12	129	0.59	0.32	1.06
INSR	Chronic ischaemic heart disease (Union#I25#I25)	Rare damaging missense (missense variants with MAF≤0.025% and REVEL score ≥ 0.25)	9.84×10^{-2}	176,170	133	715	1.17	0.97	1.41
		Rare damaging, MTR informed (missense variants with MAF≤0.025% and REVEL score ≥ 0.25, MTR <25th %ile or intergenic MTR < 50th %ile)	5.06×10^{-2}	176,170	100	506	1.25	1.00	1.54
ACVR1C	Chronic ischaemic heart disease (Union#I25#I25))	NA	NA	NA	NA	NA	NA	NA	NA
PDE3B	Chronic ischaemic heart disease (Union#I25#I25)	Rare damaging, MTR informed (missense variants with MAF≤0.025% and REVEL score ≥ 0.25, MTR <25th %ile or intergenic MTR < 50th %ile)	4.98×10^{-2}	176,170	38	335	0.71	0.51	1.00
		Non-synonymous recessive (non-synonymous variants with MAF≤1%)	8.57×10^{-2}	176,170	8	96	0.52	0.25	1.08

Abbreviations: QV, qualifying variant; LCI, lower 95% confidence interval; UCI, upper 95% confidence interval; NA, not available.

Supplementary Table 11: Leave one out analysis results for the most significant single variant in significant genes.

Category	Gene	Variant	chr	pos	Major Allele	Minor Allele	Consequence	MAF	Gene-based p-value	Gene-based p value after dropping the variant
pLoF	*PLIN4* p.Q372X	rs201581703	19	4512804	G	A	Stop gained	0.158%	5.86×10^{-7}	1.79×10^{-4}
pLoF	*PLIN1* p.T338DfsX51	rs750619494	15	89667122	CTTCTGC AGGGT	C	Frameshift variant	0.029%	9.82×10^{-9}	9.29×10^{-4}
pLoF	*INSR* p.525RX	rs1599937180	19	7168005	G	A	Stop gained	0.001%	6.21×10^{-7}	2.61×10^{-4}
Moderate	*ACVR1C* p.I195T	rs56188432	2	157550353	A	G	Missense variant	0.208%	4.57×10^{-7}	0.026
pLoF+ Moderate	*ACVR1C* p.I195T	rs56188432	2	157550353	A	G	Missense variant	0.208%	1.68×10^{-7}	0.011
pLoF	*PDE3B* p.R783X	rs150090666	11	14843853	C	T	Stop gained	0.095%	1.41×10^{-6}	0.493

Abbreviations: pLOF, predicted loss of function; chr, chromosome; pos, position (b38); MAF, minor allele frequency; Pval, STAAR-O p-value; Beta, effect size; SE, standard error; RR, reference/reference genotype; RA, reference/alternate genotypes; AA alternate/alternate genotypes.

Supplementary Table 12. Phenotypes used for phenotypic associations in UK Biobank. Sex (for sex-combined analyses), sequencing batch (50K vs. 150K), genotyping array, and 10 genetic principal components were included as covariates in association analyses.

Outcome	Cases, N	Non-cases (for case-control studies) or participants (for continuous traits studies) in sub-study, N	Adjustments for the phenotype
BMI	NA	184,291	RB-INV transformed
Gynoid fat	NA	178,143	logn transformed, adjusted for age and logn total body fat, RB-INV of residuals within each sex separately
Android fat	NA	178,143	logn transformed, adjusted for age and logn total body fat, RB-INV of residuals within each sex separately
Leg fat	NA	178,143	logn transformed, adjusted for age and logn total body fat, RB-INV of residuals within each sex separately
Arm fat	NA	178,143	logn transformed, adjusted for age and logn total body fat, RB-INV of residuals within each sex separately
Trunk fat	NA	178,143	logn transformed, adjusted for age and logn total body fat, RB-INV of residuals within each sex separately
HbA1c	NA	175,778	RB-INV transform within aliquots, excluded prevalent T2D cases.
HDL cholesterol	NA	161,239	RB-INV transform within aliquots
LDL cholesterol	NA	146,020	RB-INV transform within aliquots, statin users were excluded
Triglycerides (TG)	NA	175,271	ln transformed, RB-INV transform within aliquots
TG/HDL ratio	NA	161,102	RB-INV transform within aliquots
Type 2 Diabetes	12875	171,462	According to the previously published UKBB probable T2D algorithm (27631769) based on baseline self-reported diabetes or medications, in addition to evidence from electronic health records (Hospital Episode Statistics or Death Registration) consistent with T2D (International Statistical Classification of Diseases and Related Health Problems Tenth Revision code E11)
Coronary Heart Disease	11821	172,516	Based on CALIBER working group's definition based on primary and secondary care records in UK Biobank

Abbreviations: BMI, body mass index; HDL high-density lipoproteins; LDL low-density lipoproteins; RB-INV, rank-based inverse normal transformation; NA, not available.

Supplementary Figure 1: Regional association plots of the overall and statistically-decomposed signals at the *CALCRL*, *PLIN1*, *PDE3B* and *ACVR1C* genes. Plots were drawn using LocusZoom [6]. Joint meta-analysis models using GCTA [1] were used at each locus to assess how many independent signals were present. Then, at each locus each signal was statistically-decomposed from others by estimating associations of all variants in the region adjusted for all other index variants at the region. Fine-mapping of each signal was performed using a Bayesian approach [7].
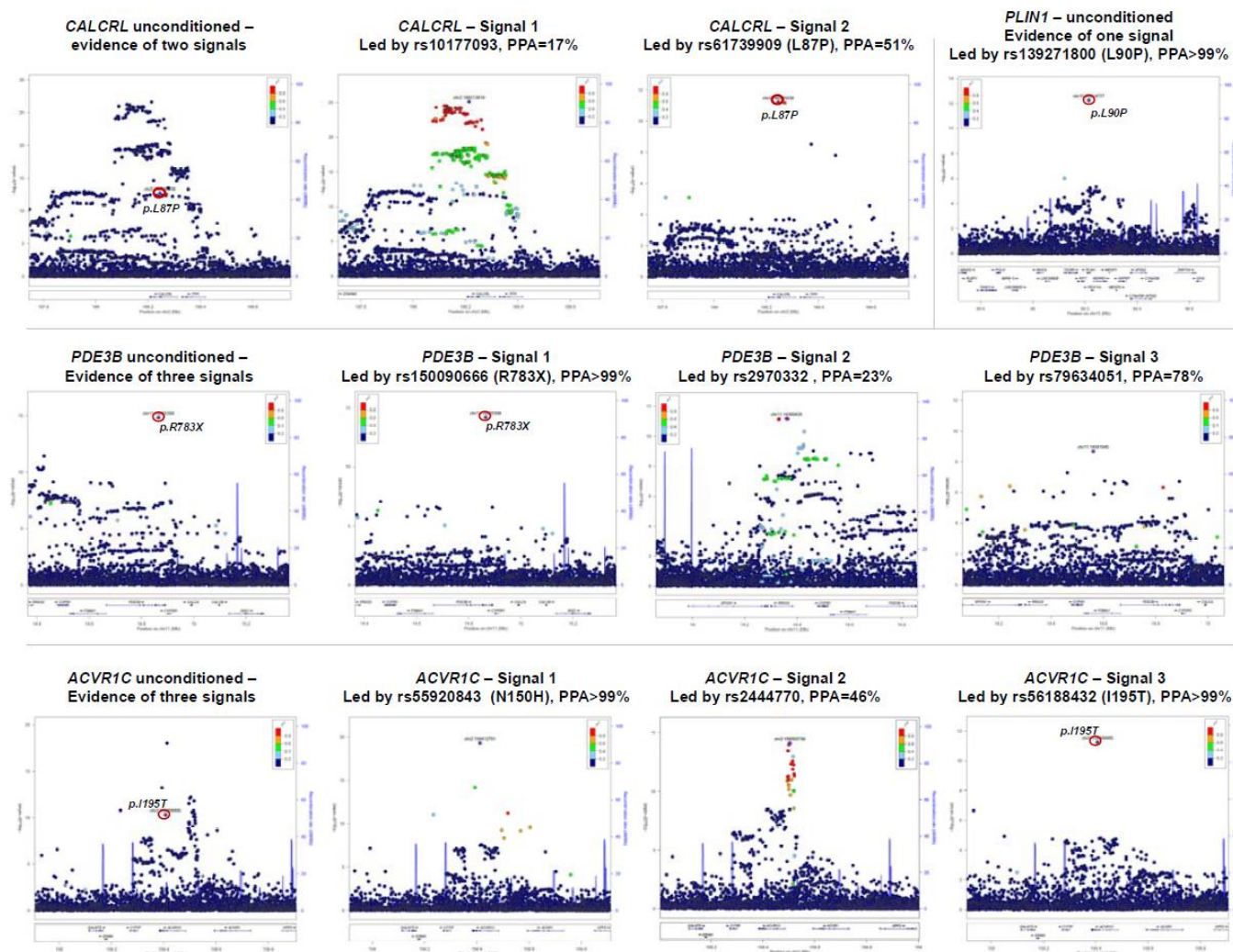
Supplementary Figure 2: Association of the significant genes with other body fat distribution or cardiometabolic trait related phenotypes in UK Biobank for (a) continuous phenotypes and (b) binary phenotypes. There was no rare predicted loss of function variant carriers for *INSR* in coronary heart disease (CHD) cases in women-only analyses. Abbreviations: pLoF, predicted loss of function; OR, odds ratio; WHRadjBMI; waist-to-hip ratio adjusted for body mass index; BMI, body mass index; TG, triglycerides; HD; high density lipoprotein, LDL low-density lipoprotein; TG/HDL, triglyceride to high density lipoprotein ratio; T2D, type 2 diabetes; CHD, coronary heart disease.

a.
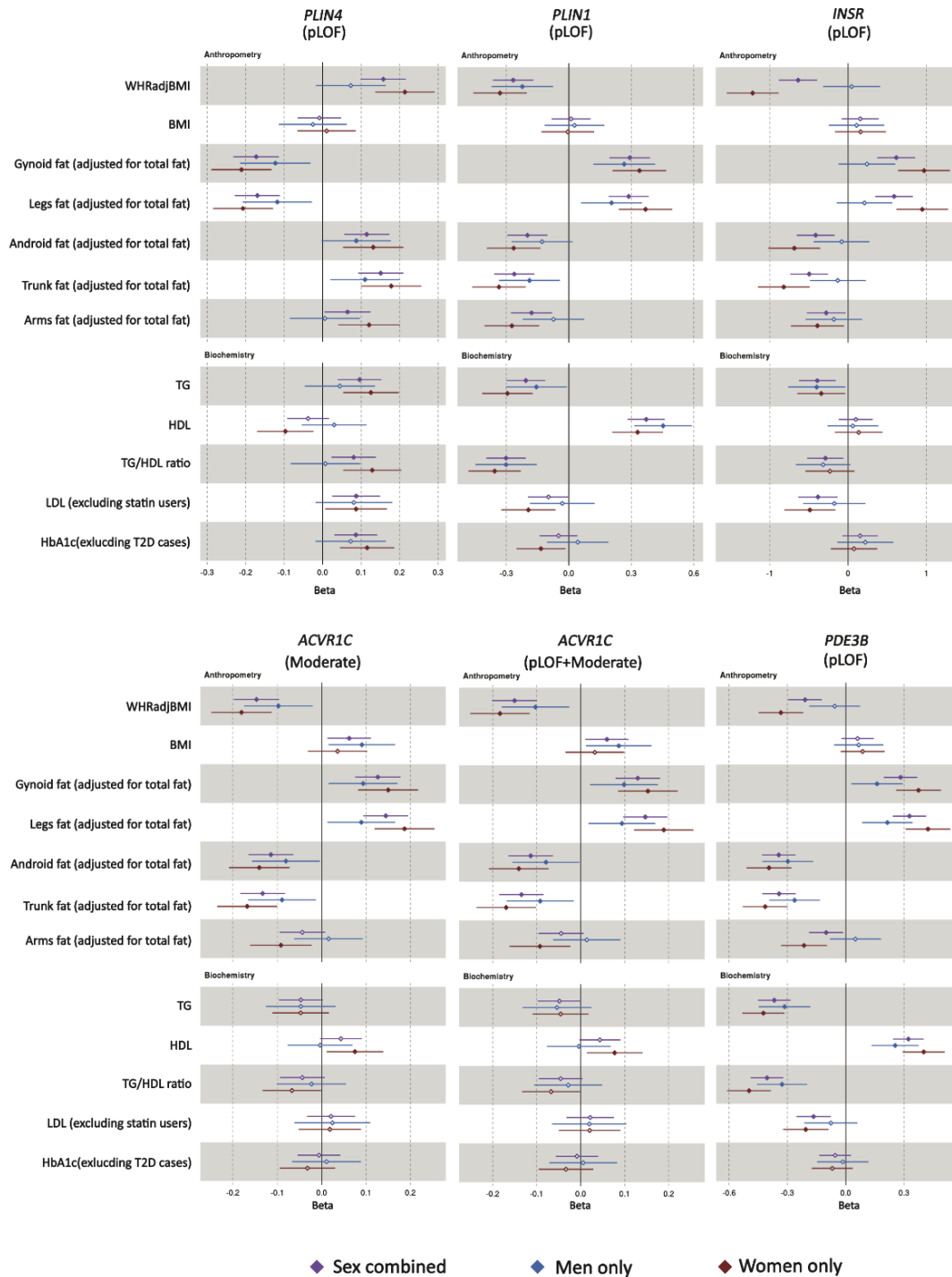
b.
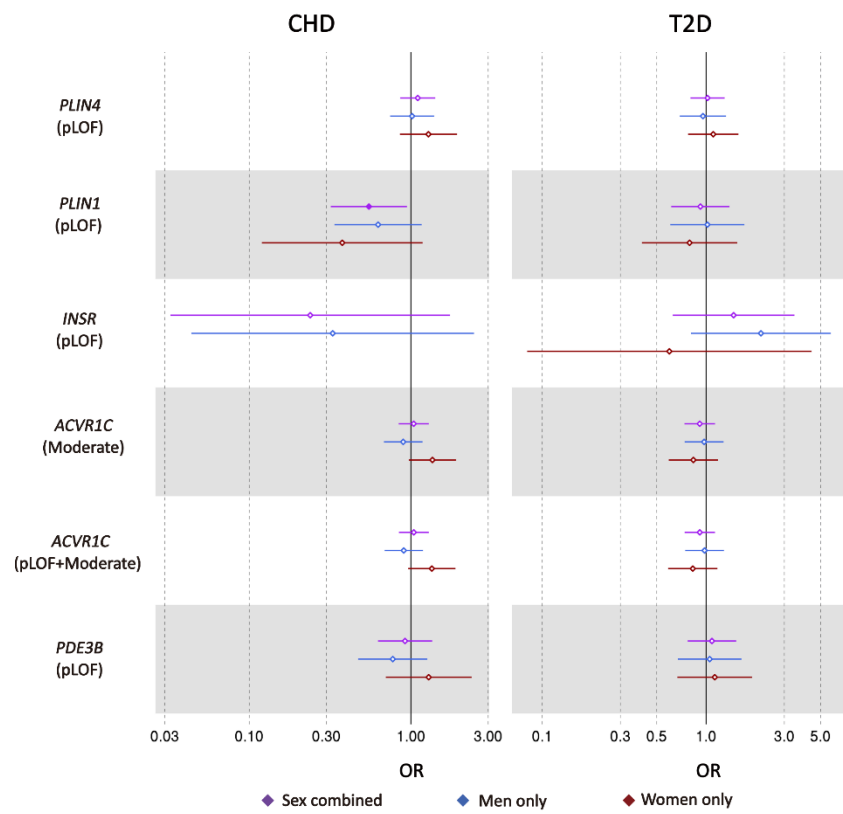
Supplementary Note 1: Genomic context analyses at the *PLIN1*, *ACVR1C*, *PDE3B* and *CALCRL* loci.

Fine-mapping analyses provided strong statistical evidence for the causal association of rare nonsynonymous variants of *CALCRL, PLIN1, PDE3B* and *ACVR1C*.

At *PLIN1*, there was evidence of only one signal led by the rare p.L90P variant (rs139271800; Supplementary Figure 1), which was the only variant in the 99% credible set (PPA>99%; Supplementary Table 3).

At *ACVR1C*, there was evidence of three distinct signals (Supplementary Figure 1, Supplementary Table 3). The rare p.I195T variant led one of the secondary signals at this region and was the only variant in the 99% credible set (PPA>99%; Supplementary Table 3). In addition, the primary signal at this region was led by a low-frequency missense variant in *ACVR1C* (rs55920843, p.N150H), which also had the highest posterior probability in fine-mapping of this signal (PPA>99%; Table 1). Hence, fine-mapping of conditionally-independent signals at this locus converges on *ACVR1C* as causal gene for body fat distribution and p.I195T and p.N150H as causal variants for the respective association peaks.
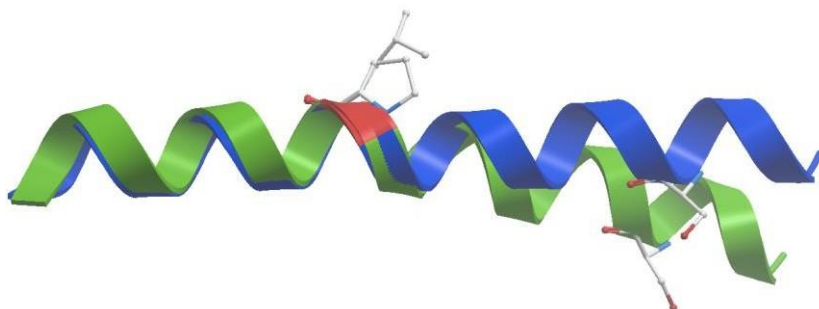
At *PDE3B*, there was evidence of three signals, the strongest of which was led by the rs150090666 p.R783X nonsense variant in *PDE3B*, which was the only variant in the 99% credible set (PPA>99%; Supplementary Figure 1, Supplementary Table 3).
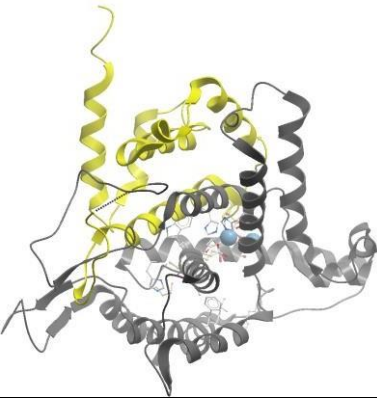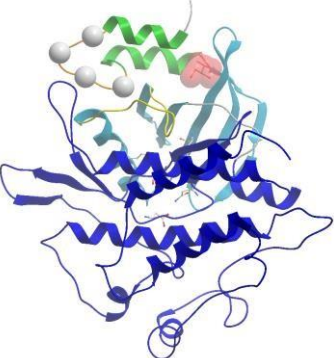
At *CALCRL*, there was evidence of two conditionally-independent signals (Supplementary Figure 1, Supplementary Table 3), led by the rs10177093 common variant and by the rare p.L87P variant, respectively. Fine-mapping at the latter signal yielded a 99% credible set including only two variants, rs61739909 (*CALCRL* p.L87P, posterior probability of casual association [PPA]=51%) and rs180960888 (intronic to *CALCRL*, PPA=48.5%). Hence, p.L87P is the most likely causal variant and *CALCRL* the most likely causal gene for this signal.

Supplementary Note 2: Genomic context analyses at the *ABHD15*, *PYGM*, *PLCB3* and *FNIP1* loci.

In the main analysis, we found associations of rare nonsynonymous variants in *ABHD15* and *PYGM* for which genomic context analyses were not consistent with a causal association. At *ABHD15*, conditional analyses revealed two distinct association signals tagged by the rs62070804 and rs561089333 index-variants respectively (Supplementary Table 4). The rare nonsynonymous rs141385558 p.G147D variant was not among these index variants and its association was greatly attenuated after adjusting for the two independent index variants ($p_{conditional}$=0.00019; Supplementary Table 1). At *PYGM*, there was a complex association pattern with evidence of up to 12 distinct signals (Supplementary Table 4). The rare nonsense rs116987552 p.R50X variant was not among these 12 index variants and its association was greatly attenuated after adjusting for these 12 index variants ($p_{conditional}$=0.00037; Supplementary Table 1). In the secondary analyses, we found associations of rare nonsynonymous variants in *PLCB3* (both in experiment-level p-value and sex-specific analyses) and *FNIP1* (sex-specific analyses) for which genomic context analyses were not consistent with a causal association. At *PLCB3*, there was evidence of up to ten independent signals (Supplementary Table 4) but the p.V806I variant was not among those and adjusting for the conditionally-independent index variants greatly attenuated its association ($p_{conditional}$>0.10; Supplementary Table 1). At *FNIP1* there was evidence of only one signal but the p.R518Q missense variant was not the lead variant (Supplementary Table 4). Adjusting for the lead variant attenuated the signal ($p_{conditional}$=3.8×10^{-7}; Supplementary Table 1) and the variant had low posterior probability in the fine-mapping analysis (PPA=8.7%).

Supplementary Note 3: Predictions regarding the variants identified through single marker analysis.

| Gene, allele Gene product	Information on gene function, structural modelling and biological insights of associations reported in this study
PLIN1 p.L90P Perilipin 1	Perilipin 1 is a constitutive lipid droplet-associated protein predominantly expressed in adipocytes, where it is necessary for optimal triglyceride storage and for the precisely regulated release of fatty acids from the droplet [8]. Perilipin 1 has a well-established role as a negative regulator of intracellular lipolysis [9,10]. Rare loss-of-function mutations in *PLIN1* cause autosomal dominant forms of partial lipodystrophy with lack of gluteo-femoral and leg fat, insulin resistance, dyslipidemia and type 2 diabetes [11]. Leucine 90 is conserved in *Mammalia* and *Sauria* and replaced conservatively in lower species (*Inset Figure 1*). It lies at the N-terminal edge of the highly-conserved PAT domain responsible for the interaction with hormone sensitive lipase, the enzyme that catalyzes intracellular diglyceride hydrolysis [12]. Although the structure of this region is unknown, it is predicted to be highly helical and the substitution of leucine with proline at position 90 is predicted to break the helix, introducing a sharp kink (*Inset Figure 2*). Thus, p.L90P, which is associated with lower waist- to-hip ratio, higher overall adiposity, and lipid levels in our human genetic studies, may affect intracellular lipolysis by impacting on perilipin 1 interaction with hormone sensitive lipase. Our results show that nonsynonymous variation in this gene influences fat distribution and lipid levels in the general population, adding to the notion of shared genetic mechanisms between severe and subtle forms of human lipodystrophy [13]. *Inset Figure 1*. Sequence alignment of perilipin 1 segments from representative species and human perilipin 2, 3 and 5. Perilipin 4 is not included due to divergence and multiplication of its N-terminus. The structure of the segment is modelled in *Inset Figure 2*. Arrows indicate the mutated L90 (red) and phosphorylated S81 (black). *Inset Figure 2*. Comparison of models of the native (blue) and mutated (green) fragment of perilipin 1 including amino acids 77 through 99. Built on the helical fragment of Protein Data Bank structure 4BJM/205-228 and superposed for the minimal root-mean-square deviation of the backbone (red) between L90 and P90. Their side chains are displayed together with S81 in ball and stick representation.

|	
PDE3B p.R783X Phosphodiesterase 3B	Phosphodiesterase 3B is a membrane bound phosphodiesterase highly expressed in adipocytes, where it has been implicated in terminating intracellular lipolysis in response to insulin by degrading cyclic adenosine monophosphate [14]. Phosphodiesterase 3B null mice manifest enhanced intracellular lipolysis, lower fat mass but higher insulin resistance [15]. The premature stop codon generated by p.R783X falls within the proximal half of the catalytic domain of phosphodiesterase 3B, removing most of its Mg^{2+} binding site (*Inset Figure 3*). Hence, this rare null variant, associated in our human genetic studies with lower waist-to-hip ratio, higher levels of peripheral adiposity and lower blood pressure and triglycerides is expected to result in a loss of catalytic function of phosphodiesterase 3B. If the protein is expressed, it could be embedded in the membrane through its intact N-terminal 6 membrane spanning domains and impair the phosphodiesterase 3B signalling complex [16] in a dominant-negative manner. Therefore, our data provide evidence of causal link between the loss of phosphodiesterase 3B function and greater peripheral fat, more favourable fat distribution and lower blood pressure and atherogenic lipids in humans. The effect size of this null allele on waist-to-hip ratio is over 6-fold greater than that of the strongest alleles found in GWAS of common variants [17]. Inset Figure 3. Structure of the catalytic domain of PDE3B (Protein Data Bank coordinates 1SO2 [18]) with an inhibitor in the active site (Protein Data Bank coordinates 1ISO2([19])). The mutation R783X removes the protein part highlighted in grey. The N-terminus at the top of the figure is preceded by a 6 trans membrane helical domain. Inhibitor and active site residues are in ball and stick representation and the two blue balls indicate Mg^{2+} ions.
ACVR1C p.I195T Activin A Receptor Type 1C	The Activin A Receptor Type 1C is type I member of the family of transforming growth factor beta receptors transmitting signals from extracellular ligands to nuclear transcription. ACVR1C downregulates the key fat storage and glucose metabolism regulator peroxisome proliferator-activated receptor gamma [20]. ACVR1C inhibits β-adrenergic signalling, mitochondrial biogenesis, lipid oxidation, and intracellular lipolysis in adipocytes [20]. The *Inset Figure 4* shows a structural model of the intracellular part of ACVR1C. It can be seen that I195 forms a hinge between the N-terminal regulatory GS-domain and the kinase. Its side chain is tightly packed against both the kinase and the GS-domain. The serine/threonine epitope in the phosphorylation loop of the GS-domain is wedged in the active site between the kinase N- and C- lobes blocking access to the active site. Upon activation (phosphorylation), the GS-domain liberates the active site and interacts with its SMAD protein substrates. I195 is expected to be involved in any mutual GS- and kinase domain movement. Its side chain is buried in a hydrophobic environment and the change from aliphatic to polar residue should be significant. I195 is strictly conserved in all orthologues and in most metazoan paralogues including the 6 other human ones (*Inset Figure 5*). The rare replacements by different aliphatic amino acids (L, V) are very conservative. The mutation may influence kinase regulation as well as interaction with SMADs. *Inset Figure 4.* Model of ACVR1C stabilized in its inactive conformation built according to the structure of TGFBR1 (Protein Data Bank coordinates 1B6C [21]). The N- terminus pointing to the membrane is on the top. The kinase domain is colored in blue, its N- and C-lobes distinguished in light and dark with the catalytic side- chains displayed in ball and stick and the activation loop in yellow. The regulatory GS-domain is in green with the phosphorylation epitope in orange and the alpha carbons of the residues to be phosphorylated upon activation highlighted by balls. The mutated L195 in ball and stick and space filling representation is in red.

Inset Figure 5. Alignment of AVCR1C sequence segments from representative species and the human paralogues from TGF-beta family. The segment covers the transmembrane domain (brown), linker (yellow), GS-domain (green) with the phosphorylation loop (orange) followed by a hinge (red) and the first beta-strand of the kinase (blue). The latter four elements can be seen in 3D in *Inset Figure 4* using the same color coding. Arrow indicate the mutated I195.

CALCRL p.L87P Calcitonin receptor-like	Calcitonin receptor-like receptor is a G-protein coupled receptor which requires association with one of the receptor activity-modifying proteins 1-3 (RAMP1-3) for ligand binding and receptor activation [22]. When associated with RAMP1, it serves as a receptor for calcitonin gene-related peptide (CGRP), whereas when associated with RAMP2-3 it functions as a receptor for adrenomedullin which is most widely recognized as a vasoactive peptide [23,24]. Mouse knockouts of adrenomedullin [25] and CALCRL [25] are embryonic lethal. However, adrenomedullin, CALCRL and RAMP2-3 are all expressed in human adipocytes where adrenomedullin has been shown to stimulate intracellular lipolysis [26]. Leucine 87 is not a conserved residue and is replaced by proline in several species (*Inset Figure 6*). The mutation is located at the tip of a strand in a beta-hairpin next to C88 and C127, both of which are strictly conserved (*Inset Figures 6-7*). The existence of the neighboring disulfide cross-link which is strictly conserved indicates that the orientation of the hairpin is important and it is indeed in close contact with RAMP2. The mutation may partially destabilize the beta-sheet, leading to a slight readjustment of the hairpin, and its interaction with adrenomedullin. The effect on ligand binding will however be indirect and probably mild in the complex with RAMP2 and adrenomedullin. However, the effect might be stronger when the receptor forms a complex with RAMP1 or 3 and interacts with different ligands. The association of p.L87P with lower waist-to-hip ratio coupled with the high expression of the *CALCRL* gene in adipose tissue point to a possible role in adipocyte biology of this G-protein coupled receptor.
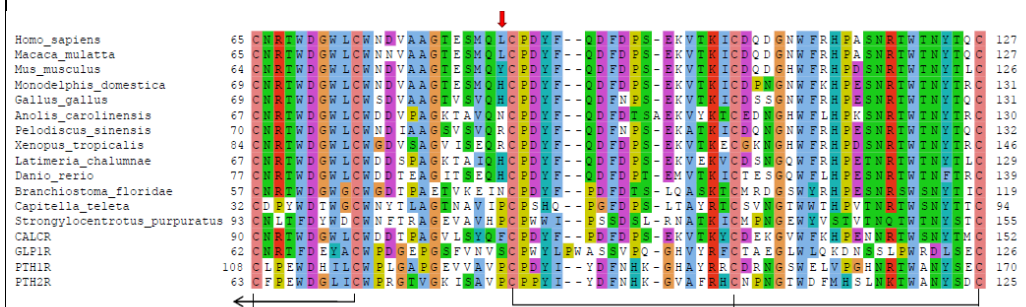
Inset Figure 6. Sequence alignment of CALCRL segments from representative species and the closest human homologues. The disulfide bonds are indicated by black connectors and the mutated L87 by a red arrow. The fragment covers the beta-barrel in *Inset Figure 7*.
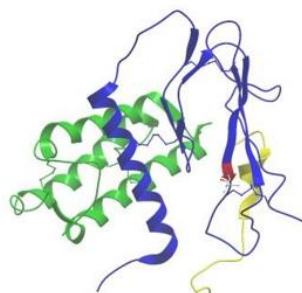
Inset Figure 7. Structure of the extracellular portion of the complex between CALCRL (blue), RAMP2 (yellow) and adrenomedullin (green). Extensions of the C-terminus of CALRL and the N-terminus of RAMP2 (not shown in this model) constitute the trans-membrane and intracellular domains of CALCRL and RAMP2. The position of L87 is in red and its side-chain in ball and stick representation. The side chains of the conserved structure stabilizing cysteines are also shown. Protein Data Bank coordinates 4RWF [27] were used for modelling.

REFERENCES

1.   Yang J, Lee SH, Goddard ME, Visscher PM. GCTA: a tool for genome-wide complex trait analysis. *Am J Hum Genet*. Jan 07 2011;88(1):76-82. doi:10.1016/j.ajhg.2010.11.011

2.   Li X, Li Z, Zhou H, et al. Dynamic incorporation of multiple in silico functional annotations empowers rare variant association analysis of large whole-genome sequencing studies at scale. *Nat Genet*. 09 2020;52(9):969-983. doi:10.1038/s41588-020-0676-4

3.   McLaren W, Gil L, Hunt SE, et al. The Ensembl Variant Effect Predictor. *Genome Biol*. Jun 2016;17(1):122. doi:10.1186/s13059-016-0974-4

4.   Loh PR, Tucker G, Bulik-Sullivan BK, et al. Efficient Bayesian mixed-model analysis increases association power in large cohorts. *Nat Genet*. Mar 2015;47(3):284-90. doi:10.1038/ng.3190

5.   Wang Q, Dhindsa RS, Carss K, et al. Rare variant contribution to human disease in 281,104 UK Biobank exomes. *Nature*. Aug 10 2021;doi:10.1038/s41586-021-03855-y

6.   Pruim RJ, Welch RP, Sanna S, et al. LocusZoom: regional visualization of genome-wide association scan results. *Bioinformatics*. Sep 15 2010;26(18):2336-7. doi:10.1093/bioinformatics/btq419

7.   Maller JB, McVean G, Byrnes J, et al. Bayesian refinement of association signals for 14 loci in 3 common diseases. *Nat Genet*. Dec 2012;44(12):1294-301. doi:10.1038/ng.2435

8.   Brasaemle DL, Subramanian V, Garcia A, Marcinkiewicz A, Rothenberg A. Perilipin A and the control of triacylglycerol metabolism. *Mol Cell Biochem*. Jun 2009;326(1-2):15-21. doi:10.1007/s11010-008-9998-8

9.   Granneman JG, Moore HP, Krishnamoorthy R, Rathod M. Perilipin controls lipolysis by regulating the interactions of AB-hydrolase containing 5 (Abhd5) and adipose triglyceride lipase (Atgl). *J Biol Chem*. Dec 11 2009;284(50):34538-44. doi:10.1074/jbc.M109.068478

10.   Gandotra S, Lim K, Girousse A, Saudek V, O'Rahilly S, Savage DB. Human frame shift mutations affecting the carboxyl terminus of perilipin increase lipolysis by failing to sequester the adipose triglyceride lipase (ATGL) coactivator AB-hydrolase-containing 5 (ABHD5). *J Biol Chem*. Oct 07 2011;286(40):34998-5006. doi:10.1074/jbc.M111.278853

11.   Gandotra S, Le Dour C, Bottomley W, et al. Perilipin deficiency and autosomal dominant partial lipodystrophy. *N Engl J Med*. Feb 24 2011;364(8):740-8. doi:10.1056/NEJMoa1007487

12.   Sztalryd C, Brasaemle DL. The perilipin family of lipid droplet proteins: Gatekeepers of intracellular lipolysis. *Biochim Biophys Acta Mol Cell Biol Lipids*. Oct 2017;1862(10 Pt B):1221-1232. doi:10.1016/j.bbalip.2017.07.009

13.   Lotta LA, Gulati P, Day FR, et al. Integrative genomic analysis implicates limited peripheral adipose storage capacity in the pathogenesis of human insulin resistance. *Nat Genet*. 01 2017;49(1):17-26. doi:10.1038/ng.3714

14.   DiPilato LM, Ahmad F, Harms M, Seale P, Manganiello V, Birnbaum MJ. The Role of PDE3B Phosphorylation in the Inhibition of Lipolysis by Insulin. *Mol Cell Biol*. Aug 2015;35(16):2752-60. doi:10.1128/MCB.00422-15

15.   Degerman E, Ahmad F, Chung YW, et al. From PDE3B to the regulation of energy homeostasis. *Curr Opin Pharmacol*. Dec 2011;11(6):676-82. doi:10.1016/j.coph.2011.09.015

16.   Wilson LS, Baillie GS, Pritchard LM, et al. A phosphodiesterase 3B-based signaling complex integrates exchange protein activated by cAMP 1 and phosphatidylinositol 3-kinase signals in human arterial endothelial cells. *J Biol Chem*. May 06 2011;286(18):16285-96. doi:10.1074/jbc.M110.217026

17.   Shungin D, Winkler TW, Croteau-Chonka DC, et al. New genetic loci link adipose and insulin biology to body fat distribution. *Nature*. Feb 12 2015;518(7538):187-196. doi:10.1038/nature14132

18.   Scapin G, Patel SB, Chung C, et al. Crystal structure of human phosphodiesterase 3B: atomic basis for substrate and inhibitor specificity. *Biochemistry*. May 25 2004;43(20):6091-100. doi:10.1021/bi049868i

19.   ter Haar E, Koth CM, Abdul-Manan N, et al. Crystal structure of the ectodomain complex of the CGRP receptor, a class-B GPCR, reveals the site of drug antagonism. *Structure*. Sep 08 2010;18(9):1083-93. doi:10.1016/j.str.2010.05.014

20.   Yogosawa S, Mizutani S, Ogawa Y, Izumi T. Activin receptor-like kinase 7 suppresses lipolysis to accumulate fat in obesity through downregulation of peroxisome proliferator-activated receptor γ and C/EBPα. *Diabetes*. Jan 2013;62(1):115-23. doi:10.2337/db12-0295

21.   Huse M, Chen YG, Massagué J, Kuriyan J. Crystal structure of the cytoplasmic domain of the type I TGF beta receptor in complex with FKBP12. *Cell*. Feb 05 1999;96(3):425-36. doi:10.1016/s0092-8674(00)80555-3

22.   Watkins HA, Chakravarthy M, Abhayawardana RS, et al. Receptor Activity-modifying Proteins 2 and 3 Generate Adrenomedullin Receptor Subtypes with Distinct Molecular Properties. *J Biol Chem*. May 27 2016;291(22):11657-75. doi:10.1074/jbc.M115.688218

23.   Mistrova E, Wiegand S, Sviglerova J, et al. Adrenomedullin and the calcitonin receptor-like receptor system mRNA expressions in the rat heart and sensory ganglia in experimentally-induced long-term diabetes. *Gen Physiol Biophys*. 2014;33(2):215-25. doi:10.4149/gpb_2013073

24.   Watkins HA, Walker CS, Ly KN, et al. Receptor activity-modifying protein-dependent effects of mutations in the calcitonin receptor-like receptor: implications for adrenomedullin and calcitonin gene-related peptide pharmacology. *Br J Pharmacol*. Feb 2014;171(3):772-88. doi:10.1111/bph.12508

25.   Dackor RT, Fritz-Six K, Dunworth WP, Gibbons CL, Smithies O, Caron KM. Hydrops fetalis, cardiovascular defects, and embryonic lethality in mice lacking the calcitonin receptor-like receptor gene. *Mol Cell Biol*. Apr 2006;26(7):2511-8. doi:10.1128/MCB.26.7.2511-2518.2006

26.   Dong Y, Betancourt A, Belfort M, Yallampalli C. Targeting Adrenomedullin to Improve Lipid Homeostasis in Diabetic Pregnancies. *J Clin Endocrinol Metab*. 09 01 2017;102(9):3425-3436. doi:10.1210/jc.2017-00920

27.   Booe JM, Walker CS, Barwell J, et al. Structural Basis for Receptor Activity-Modifying Protein-Dependent Selective Peptide Recognition by a G Protein-Coupled Receptor. *Mol Cell*. Jun 18 2015;58(6):1040-52. doi:10.1016/j.molcel.2015.04.018